THE JOURNAL OF BIOLOGICAL CHEMISTRY VOL. 283, NO. 3, pp. 1660–1669, January 18, 2008
Printed in the U.S.A.

Structural and Functional Characterization of the TRI101 Trichothecene 3-*O*-Acetyltransferase from *Fusarium sporotrichioides* and *Fusarium graminearum*

KINETIC INSIGHTS TO COMBATING FUSARIUM HEAD BLIGHT[*S]

Received for publication, July 13, 2007, and in revised form, October 1, 2007 Published, JBC Papers in Press, October 8, 2007, DOI 10.1074/jbc.M705752200

Graeme S. Garvey[‡], **Susan P. McCormick**[§], **and Ivan Rayment**[‡1]

From the [‡]*Department of Biochemistry, University of Wisconsin, Madison, Wisconsin 53706 and the* [§]*Mycotoxin Research Unit, USDA/ARS, National Center for Agricultural Utilization Research, Peoria, Illinois 61604*

Fusarium **head blight (FHB) is a plant disease with serious economic and health impacts. It is caused by fungal species belonging to the genus *Fusarium* and the mycotoxins they produce. Although it has proved difficult to combat this disease, one strategy that has been examined is the introduction of an indigenous fungal protective gene into cereals such as wheat barley and rice. Thus far the gene of choice has been *tri101* whose gene product catalyzes the transfer of an acetyl group from acetyl coenzyme A to the C3 hydroxyl moiety of several trichothecene mycotoxins. *In vitro* this has been shown to reduce the toxicity of the toxins by ~100-fold but has demonstrated limited resistance to FHB in transgenic cereal. To understand the molecular basis for the differences between *in vitro* and *in vivo* resistance the three-dimensional structures and kinetic properties of two TRI101 orthologs isolated from *Fusarium sporotrichioides* and *Fusarium graminearum* have been determined. The kinetic results reveal important differences in activity of these enzymes toward B-type trichothecenes such as deoxynivalenol. These differences in activity can be explained in part by the three-dimensional structures for the ternary complexes for both of these enzymes with coenzyme A and trichothecene mycotoxins. The structural and kinetic results together emphasize that the choice of an enzymatic resistance gene in transgenic crop protection strategies must take into account the kinetic profile of the selected protein.**

Fusarium head blight (FHB)[2] is a plant disease with serious economic and health consequences (1, 2). The disease is caused by several species of the fungus *Fusarium* that reduce grain yields and contaminate the grains with trichothecene mycotoxins such as deoxynivalenol, nivalenol, and T-2 toxin. In the United States and Europe, deoxynivalenol (DON) and 15-acetyl-DON are the primary grain contaminants, where these are produced by strains of *Fusarium graminearum* (3, 4). Although considerable effort has been devoted to overcoming this agricultural problem, at present there is no satisfactory way of combating these pathogens or their associated toxins.

The trichothecene mycotoxins are a structurally diverse group of sesquiterpene epoxides that inhibit protein synthesis in eukaryotes (5). They all contain a 12,13-epoxytrichothecene skeleton, but differ in various side chain substitutions. Two types of toxins have been defined according to substitution at C8 (Fig. 1) (6). Type A carry a non-ketone side chain, or no side chain at all, whereas in Type B this position is occupied by a ketone functional group. T-2 toxin is an A type trichothecene with an ester-linked isovaleryl group at C8, whereas DON and nivalenol (NIV) are both B type trichothecenes with a ketone moiety at C8 and are further differentiated by their substitution patterns at C4 (Fig. 1).

The nature of the side chains can have drastic effects on the cytotoxicity of these compounds. As much as 5×10^3-fold difference in LC_{50} has been observed among these toxins (7). Significantly, the presence of an acetyl group attached to the C3 hydroxyl lowers the toxicity considerably and has been implicated as the self-protection mechanism in the trichothecene mycotoxin producing *Fusarium* species (8).

The trichothecene biosynthetic pathway for the T-2 toxin producing strain, *Fusarium sporotrichioides,* has been established from gene disruption mutants and the analysis of intermediate trichothecene metabolites (Refs. 9 and 10 and references cited therein). The pathway begins with the cyclization of farnesyl pyrophosphate by trichodiene synthase, *tri5* (11, 12). The next enzyme in the pathway, TRI4, catalyzes multiple oxygenations to produce the toxic intermediate, isotrichodermol (7, 13). Thereafter, TRI101 catalyzes the acetylation of the C3

* This work was supported by National Institutes of Health Grant AR35186 (to I. R.) and the United States Department of Agriculture under Agreement FY06-RA-098. This is a cooperative project with the United States Wheat & Barley Scab Initiative. Use of the Structural Biology BM19 beamline Argonne National Laboratory Advanced Photon Source was supported by the United States Department of Energy, Office of Energy Research Contract W-31-109-ENG-38. The costs of publication of this article were defrayed in part by the payment of page charges. This article must therefore be hereby marked "*advertisement*" in accordance with 18 U.S.C. Section 1734 solely to indicate this fact.

[S] The on-line version of this article (available at http://www.jbc.org) contains supplemental Figs. S1–S3.

The atomic coordinates and structure factors (code 2ZBA, 2RKT, 3B30, 2RKV, and 3B2S) have been deposited in the Protein Data Bank, Research Collaboratory for Structural Bioinformatics, Rutgers University, New Brunswick, NJ (http://www.rcsb.org/).

[1] To whom correspondence should be addressed: Dept. of Biochemistry, 433 Babcock Dr., Madison, WI 53706. Tel.: 608-262-0437; Fax: 608-262-1319; E-mail: ivan_rayment@biochem.wisc.edu.

[2] The abbreviations used are: FHB, *Fusarium* head blight; DON, deoxynivalenol; FsTRI101, TRI101 from *F. sporotrichioides*; FgTRI101, TRI101 from *F. graminearum*; MEPEG2K, methylether poly(ethyleneglycol) 2000; NIV, nivalenol; TCEP, tris(2-carboxyethyl)phosphine hydrochloride; MOPS, 3-(*N*-morpholino)propanesulfonic acid.

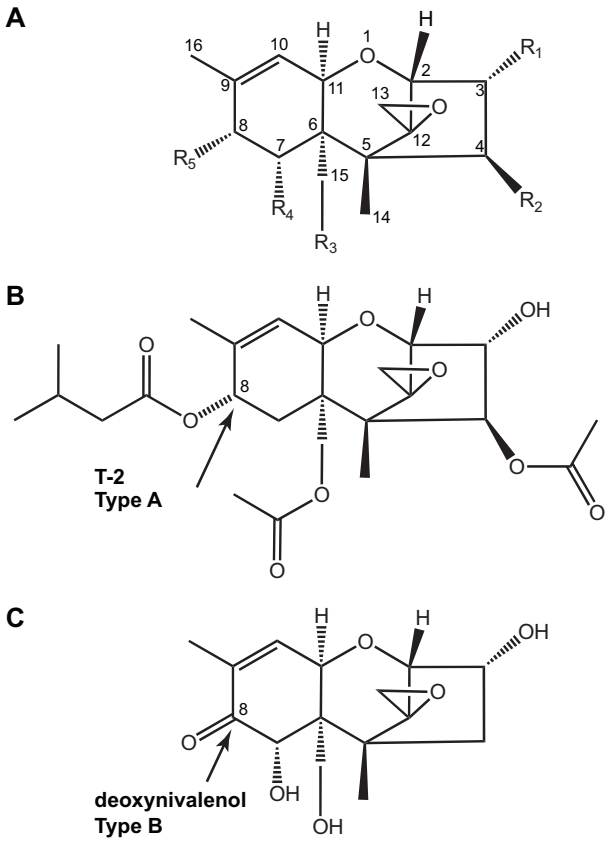

FIGURE 1. **Schematic representation of the trichothecene mycotoxin core ring structure and structures for T-2 toxin and DON (for isotrichodermaol R^1 = OH, R^2, R^3, R^4, and R^5 = H).**

hydroxyl group, which has been demonstrated to lower the toxicity of trichothecene mycotoxins 100-fold (7, 13). The acetylation at C3 has been proposed to protect the *Fusarium* through the remainder of the biosynthetic pathway (8). Indeed, TRI101 will acetylate and reduce the toxicity of the final products of the biosynthetic pathway including T-2, NIV, and DON (13). The last step in the biosynthetic pathway is removal of the protecting C3 acetyl group before being secreted by the organism (14, 15).

Control of the toxicity of trichothecene mycotoxins by modification of the C3 hydroxyl moiety has been identified as a resistance mechanism to FHB and DON. In *Arabidopsis thaliana* addition of a glucose moiety to the C3 hydroxyl group of DON and 15-ADON by a glucosyltransferase has been shown to reduce their toxic effects (16). Likewise, modification of the C3 hydroxyl group to a ketone by a soil bacterium in the *Agrobacterium-Rhizobium* group reduced DON toxicity 10-fold (17). For these reasons, enzymes that modify the C3 position have proved attractive targets for the development of FHB transgenic resistance strategies.

The *tri101* gene from *F. sporotrichioides* has been isolated and transgenically inserted into yeast (18), tobacco (19), wheat (20), and barley (21). Likewise, the *tri101* gene from *F. graminearum* has been transgenically inserted into *Saccharomyces pombe* (13) and rice (22). In laboratory scale tests *tri101* consistently provided protection against FHB, although direct comparisons are difficult. Unfortunately, field trials of transgenic wheat and barley expressing the *tri101* gene from *F. sporotrichioides* did not show resistance to *F. graminearum*. It was concluded that the intense disease pressure in the field trials overwhelmed the resistance provided by FsTri101 and perhaps was compounded by the use of a *tri101* gene from a T-2 producing organism rather than one from a DON producing *Fusarium* strain (21).

At the time the transgenic strains were prepared it was unknown whether there might be enzymatic differences between TRI101 orthologs from different sources. The TRI101 acetyltransferase from *F. sporotrichioides* was assessed for its ability to acetylate the C3 position of different trichothecene myctoxins, but the kinetic rate constants were not determined (13, 18–22). Given the structural differences between T-2, DON, and isotrichodermol, it would have been reasonable to expect differences in the kinetic profiles for TRI101 from different organisms. Indeed, as demonstrated here, there are clear differences in activity that would have supported an alternative choice for the construction of transgenic species.

We present here structural and kinetic data for two TRI101 orthologs isolated from *F. sporotrichioides* (FsTRI101) and from *F. graminearum* (FgTRI101). The three-dimensional structures of FsTRI101 and FgTRI101 have been determined together with a series of ternary complexes with CoA and T-2 and DON. In addition, their kinetic profiles toward A and B type trichothecene mycotoxins have been measured. The large variation in K_m between these orthologs can be explained by differences in their active sites. Finally, a mechanism for catalysis is proposed. The structural and kinetic results emphasize that the choice of an enzymatic resistance gene in transgenic crop protection strategies must take into account the kinetic profile of the selected protein.

EXPERIMENTAL PROCEDURES

Plasmid and Strain Construction—All cloning was performed in *Escherichia coli* strain Top10. The *tri101* gene (AF127176) from *F. sporotrichioides* was amplified using forward primer 5′-GCTAGCATGGCCGCAACAAGCAGCACAAGCAGCCAGTCTTTTGAC-3′ and reverse primer 5′-gCTgAgCCTACCCAATATACTTTGCGTACTTTGTCCACTCCTCATCC-3′ from genomic DNA (a gift from Dr. Jaechuk Yu, University of Wisconsin, Madison, WI). The *tri101* gene from *F. graminearum* (AB000874) was isolated from genomic DNA of strain PH-1 (a gift from Dr. Nancy Keller, University of Wisconsin, Madison, WI) using forward primer 5′-GCTAGCATGGCTTTCAAGATACAGCTCGACACCCTCGG-3′ and reverse primer 5′-gCTgAgCTTAACCAACGTACTGCGCATACTTGGTCC-3′. There are no introns in the genomic genes for either enzyme. The PCR product was ligated into the Zero Blunt TOPO vector (Invitrogen) where the sequence was verified. Thereafter the wild-type *TRI101* genes were excised with restriction enzymes NheI and BlpI (New England Biolabs), and ligated into a modified pET31b (Novagen) vector that included an N-terminal His_6 tag followed by a tobacco etch virus protease cut site. The N-terminal amino acid sequence of this construct is MSYYHHHHHHDYDIPTSELYFQGASM$_1$S$_2$. where the location of the tobacco etch virus protease cleavage site is

underlined. This cloning procedure introduced three residues at the N terminus of each enzyme.

Protein Expression—TRI101 from *F. sporotrichioides* (FsTRI101) was overexpressed in *E. coli* strain Rosetta(λDE3) (Novagen). A starter culture from a single colony was grown overnight at 37 °C in LB medium supplemented with ampicillin. 10 ml of the starter culture was used to inoculate 1 liter of LB + ampicillin media. Cultures were grown at 37 °C until they reached an optical density (A_{600}) of ~1.2. Cultures were cooled to 16 °C and induced with 1 mM isopropyl β-D-thiogalactopyranoside. Cells were harvested after 24 h by centrifugation at 5,000 × *g*, flash frozen in liquid nitrogen, and stored at −80 °C.

Protein Purification of FSTRI101—10 g of cells containing FsTRI101 were re-suspended in 70 ml of a lysis buffer, which contained 50 mM potassium phosphate, 300 mM NaCl, 20 mM imidazole, 2 mM 2-mercaptoethanol, 1 tablet/50 ml of Complete Inhibitor (Roche), and 35 mg of lysozyme at pH 8.0. The cells were lysed by sonication. Cellular debris was removed by centrifugation at 40,000 × *g* for 30 min. The supernatant was loaded onto a 5-ml column of nickel-nitrilotriacetic acid-agarose (Qiagen) previously equilibrated with lysis buffer. After washing with lysis buffer, the FsTRI101 protein was eluted with a linear gradient of 20–300 mM imidazole in lysis buffer. Fractions containing FsTRI101 protein were identified using SDS-PAGE and Coomassie Blue staining and dialyzed against 10 mM HEPES, 100 mM NaCl, 0.5 mM tris(2-carboxyethyl)phosphine hydrochloride, 2 mM EDTA, pH 7.5, buffer 4 °C. The His_6 tag was removed with tobacco etch virus protease (23). The resultant protein, after passage over a further nickel-nitrilotriacetic acid column, was concentrated to ~17 mg/ml using a Centriprep YM30 concentrator (Millipore) and dialyzed against 10 mM HEPES, 20 mM NaCl, 0.5 mM tris(2-carboxyethyl)phosphine hydrochloride, pH 7.5.

Expression and Purification of TRI101 from F. graminearum—FgTRI101 was overexpressed in a similar manner to FsTRI101 except that the cells were grown in M9 minimal media (24) and CoA (Sigma) was added to 15 μM following equilibration at 16 °C and prior to induction with isopropyl β-D-thiogalactopyranoside. Inclusion of CoA increased the percentage of soluble protein. The protein was purified as above except that the final dialysis buffer contained 10 mM HEPES, 100 mM NaCl, 0.5 mM tris(2-carboxyethyl)phosphine hydrochloride, pH 7.5. The final protein concentration was 13 mg/ml.

Preparation of Selenomethionine-labeled FsTRI101 Protein—Cultures of *E. coli* strain Rosetta(λDE3) carrying plasmid encoding *FsTRi101* were grown overnight at 37 °C in M9 minimal medium (24) supplemented with ampicillin. 10 ml of the starter culture was used to inoculate 650 ml of M9 + ampicillin. Cultures were grown at 37 °C to an optical density (A_{600}) of ~1.2. Cultures were cooled to 16 °C and supplemented with 65 mg each of L-lysine, L-threonine, and L-phenyalanine, and 31 mg each of L-leucine, L-isoleucine, L-valine, and L-selenomethionine. After 30 min, expression of the *Fstri101* gene was induced with 1 mM isopropyl β-D-thiogalactopyranoside. Cells were harvested after 20 h and flash frozen in liquid nitrogen. The protein was purified as described above.

Crystallization and Structural Determination of Selenomethionine-labeled FsTRI101—Crystals of FsTRI101 were grown by hanging drop vapor diffusion at 23 °C by mixing a 1:1 solution of protein at 11.3 mg/ml that contained 4.2 mM CoA, 167 μM T-2, and 0.83% Me_2SO with 28% methylether poly(ethylene glycol) 2000 (MEPEG2K), 55 mM $CaCl_2$ buffered with 0.1 M HEPES, pH 7.5, and equilibrating against the same precipitant. Single crystals grew to 0.15 × 0.15 × 0.15 mm in 5 days. The crystals were transferred directly into a solution containing 5% glycerol, 1 mM CoA, 25 mM NaCl, 65 mM $CaCl_2$, 30% MEPEG2K, 0.1 M HEPES buffer, pH 7.5, and then stepwise into a cryoprotectant solution containing 5% glycerol, 1 mM coenzyme A (CoA), 300 mM NaCl, 70 mM $CaCl_2$, 32% MEPEG2K, 0.1 M HEPES buffer, pH 7.5. Crystals were flash frozen in liquid nitrogen.

X-ray data were collected from crystals of native and selenomethionine-substituted protein at SBC Beamline 19-BM (Advanced Photon Source, Argonne National Laboratory, Argonne, IL). The x-ray data were processed and scaled with HKL2000 (25). X-ray data collection statistics are presented in Table 1.

The structure of *F. sporotrichioides* TRI101 was solved by two wavelength MAD phasing. The program SOLVE was utilized to locate 46 of the 52 selenium atoms in the asymmetric unit and to generate initial protein phases (figure of merit 0.45) (26). Solvent flattening with RESOLVE resulted in an interpretable electron density at 2.0-Å resolution (27). Alternate cycles of manual model building and least squares refinement with the programs COOT (28) and Refmac (29) reduced the R_{factor} to 15.6% for all x-ray data from 50 to 2.0 Å. Refinement statistics are presented in Table 1.

Crystallization of FgTRI101—Crystals of FgTRI101 in the apo form and complexed with CoA, T-2, and ethyl-CoA bound were grown by hanging drop vapor diffusion in three different forms: apo crystals grew from a 1:1 mixture of enzyme at 13 mg/ml and a precipitant solution of 2.1 M sodium malonate, 100 mM MOPS, pH 6.9, at 25 °C. Single crystals grew to 0.4 × 0.3 × 0.01 mm in 30 days. These crystals were transferred into a synthetic mother liquor containing 2.4 M sodium malonate, 135 mM NaCl, 5 mM T-2, and 100 mM MOPS, pH 6.9, at 25 °C. Crystals were flash frozen in liquid nitrogen.

Crystals of the complex of FgTRI101 with CoA and T-2 mycotoxin were grown from a 1:1 mixture of enzyme at 10.4 mg/ml and a precipitant solution of 2.1 M sodium malonate, 100 mM MOPS, pH 6.9, at 25 °C, containing 4.2 mM CoA and 1.6 mM T-2 toxin. Single crystals grew to dimensions of 0.4 × 0.4 × 0.01 mm in 55 days. Crystals were flash frozen directly from the crystallization mixture.

The complex between FgTRI101 and ethyl-CoA was crystallized by vapor diffusion from a 1:1 mixture of 12.5 mg/ml enzyme and a precipitant solution of 2.1 M sodium malonate, 100 mM MOPS, pH 6.9 at 25 °C, containing 4 mM ethyl-CoA. Single crystals grew to 0.4 × 0.4 × 0.01 mm in 55 days. Crystals were flash frozen directly from the crystallization mixture.

Crystals of FgTR101 with DON and CoA bound in the active site were obtained by soaking crystals that were previously grown in the presence of T-2. These latter crystals were grown by mixing equal volumes of 8.7 mg/ml enzyme with a precipi-

TABLE 1
Statistics for x-ray data collection and structural refinement

Data collection	FsTRI101·CoA·T-2 peak	FsTRI101·CoA·T-2 inflection	FgTRI101 apo	FgTRI101·EtCoA	FgTRI101·CoA·T-2	FgTRI101·CoA·DON
X-ray source	19BM	19BM	CuKα	19BM	19BM	19BM
Space group	$P2_1$	$P2_1$	$P42_12$	$P42_12$	$P42_12$	$P42_12$
Unit cell parameters (Å,°)	a = 100.97, b = 81.97, c = 113.51, β = 109.15	a = 100.97, b = 81.97, c = 113.51, β = 109.15	a = 114.21, b = 114.21, c = 80.38	a = 123.22, b = 123.22, c = 81.31	a = 123.1, b = 123.1, c = 81.3	a = 123, b = 123, c = 81.39
Wavelength (Å)	0.97907	0.97924	1.5418	0.96411	0.97907	0.97907
Resolution range (Å)[a]	50–2.0 (2.07)	50–2.01 (2.08)	50–1.99 (2.09)	50–1.97 (2.04)	50–1.6 (1.66)	50–1.92 (1.99)
Reflections: measured	419,547	413,093	391,147	612,294	781,226	666,553
Reflections: unique	118,172	118,024	36,684	42,390	67,669	45,602
Redundancy	3.6 (2.8)	3.5 (2.6)	10.6 (3.6)	13.7 (12.6)	10.9 (4.6)	13.9 (13)
Completeness (%)	99.7 (96.8)	99.5 (93.3)	99.6 (97.2)	99.9 (99.4)	87.5 (50.1)	99.9 (99.7)
Average I/σ	13.8 (2)	15 (1.9)	17.2 (1.92)	19.7 (5.2)	20.2 (1.2)	24.9 (5.6)
R_{merge}[b] (%)	8.7 (29)	8.5 (33.0)	8.3 (53)	7.9 (24.1)	6.3 (50.3)	7.5 (25.8)
R_{work}[c] (%)		19.8 (23.2)	19.6 (26)	18.2 (18.3)	18.4 (34.8)	16.9 (18)
R_{free} (%)		25.0 (30.0)	24.4 (30.5)	20.6 (22.5)	20.8 (39.5)	20.3 (23.2)
No. protein atoms		12837	3320	3431	3458	3453
No. water molecules		912	347	326	556	427
Wilson B-value (Å^2)		21.7	22.1	17.2	18.0	17.3
Average B factors (Å^2) and No. of atoms						
Monomer A		24.5 (3,315)	22.1 (3,320)	14.5 (3,431)	14.5 (3,458)	15.5 (3,453)
Monomer B		22.0 (3,264)				
Monomer C		17.4 (3,299)				
Monomer D		27.5 (2,959)				
Ligand		24.8 (333)		24.4 (60)	20.5 (91)	34.9 (81)
Solvent		23.4 (912)	27.4 (347)	20.8 (326)	26.2 (556)	24.7 (427)
Ramachandran (%)						
Most favored		91.5	91.0	92.4	92.1	91.7
Additionally allowed		7.4	8.4	7.3	7.9	8.3
Generously allowed		0.8	0.5	0.3	0.0	0.0
Disallowed		0.3	0.0	0.0	0.0	0.0
R.M.S deviations						
Bond lengths (Å)		0.13	0.02	0.025	0.009	0.014
Bond angles (°)		1.498	1.656	1.717	1.204	1.521
Chiral		0.10	0.12	0.102	0.079	0.124
Disordered segments		Given below[d]	N-terminal-Ala^{-2} Leu^{16}–Ser^{18}, Asp^{221}–Thr^{225}, Asp^{253}–Lys^{257}, Ser^{336}–Leu^{338}	N-terminal-Ser^{-1} Asp^{221}–Pro^{226}	N-terminal-Met^{1} Gly^{220}–Val^{227}	N-terminal-Met^{1} Pro^{130}–Asp^{131}
RCSB accession codes		2ZBA	2RKT	3B30	2RKV	3B2S

[a] The values in parentheses represent the statistics for the highest resolution shell.
[b] $R_{sym} = \Sigma|I_{(hkl)} - I| \times 100/\Sigma|I_{(hkl)}|$, where the average intensity I is taken over all symmetry equivalent measurements and $I_{(hkl)}$ is the measured intensity for a given reflection.
[c] $R_{factor} = \Sigma|F_{(obs)} - F_{(calc)}| \times 100/\Sigma|F_{(obs)}|$, where R_{work} refers to the R_{factor} for the data utilized in the refinement and R_{free} refers to the R_{factor} for 5% of the data that were excluded from the refinement.
[d] The N terminus of each monomer is disordered to Ser^{10}, Phe^{11}, Gln^{10}, and Phe^{11} of chains A, B, C, and D, respectively. There are additional disordered residues in chain A between Lys^{223} and Pro^{234}; in chain B between Lys^{223} and Pro^{231}; in chain C between Ala^{223} and Ala^{233}, Ala^{376} and Asn^{377}; and in chain D between residues Ile^{222} and Trp^{238}, Lys^{254} and Lys^{264}, Arg^{284} and Thr^{293}, and Thr^{375} and Pro^{378}.

tant solution containing 4.2 mM CoA and 167 μM T-2. Single crystals grew to 0.3 × 0.3 × 0.01 mm in 25 days. These crystals were transferred into a synthetic mother liquor containing 2.4 M sodium malonate, 2.5 mM NaCl, and 20 mM DON for 24 h, then flash frozen in liquid nitrogen.

Structure Determination of FgTRI101 Apo and Complexed to Substrates—The structure FgTRI101 complexed to CoA and T-2 was solved by molecular replacement with the program MOLREP (30) starting from the model for FsTRI101. Alternate cycles of manual model building and least squares refinement with the programs COOT (28) and Refmac (29) reduced the R_{factor} to 18.4% for all x-ray data from 50 to 1.6 Å (Table 1).

The refined FgTRI101 structure bound to CoA and T-2 was used to determine the structures for apo-FgTRI101, FgTRI101 complexed to ethyl-CoA, and FgTRI101 complexed with CoA and DON. The structures were refined as before (Table 1).

Acetyltransferase Enzymatic Assay—The trichothecene 3-*O*-acetyltransferase reaction catalyzed by TRI101 was monitored by following the production of CoA in a 5,5′-dithiobis-(2-nitrobenzoic acid) coupled continuous assay (ϵ = 14150 cm^{-1} M^{-1}) (31). Reaction mixtures were prepared at 25 °C by combining 50 μl of 1.5 mM acetyl-CoA (Sigma), 0.6 mM 5,5′-dithiobis-(2-nitrobenzoic acid) (Sigma), 0.1 M potassium phosphate buffer, pH 8, with 50 μl of trichothecene toxin, 4.5% Me_2SO, 0.1 M potassium phosphate buffer, pH 8.0. For FsTRI101 the reaction was initiated by the addition of 50 μl of 82.5 ng/ml enzyme, 200 μg/ml bovine serum albumin, 0.1 M potassium phosphate buffer, pH 8. After mixing, 100 μl of the reaction mixture was transferred to a 1-cm path length cuvette and the change in absorbance at 412 nm was followed. Reactions with FgTRI101 were as described above, using a stock protein concentration of 165 ng/ml. The rates of reaction were determined at various concentrations of isotrichodermol, T-2, NIV, and DON and then fit by non-linear regression to the Michaelis-Menten equation.

RESULTS AND DISCUSSION

Tertiary Structure of TRI101—The crystal structures of apo FgTRI101, a binary complex of FgTRI101 with ethyl-CoA, a ternary complex of FgTRI101 bound to CoA and DON, and

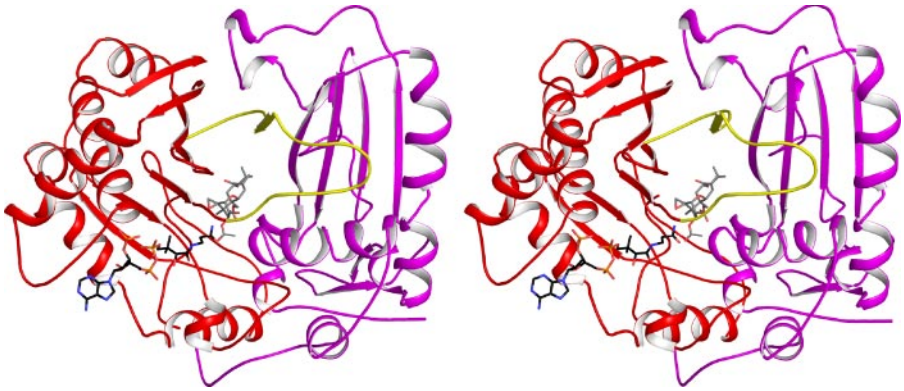

FIGURE 2. **Stereo ribbon representation of FgTRI101 complexed with CoA and DON.** The N- and C-terminal domains are colored *magenta* and *red*, respectively, and the domain swapped β-strand 12 is colored *yellow*. Bound ligands CoA and DON are colored *black* and *gray*, respectively. Figs. 2–6 were prepared with the program Pymol (39).

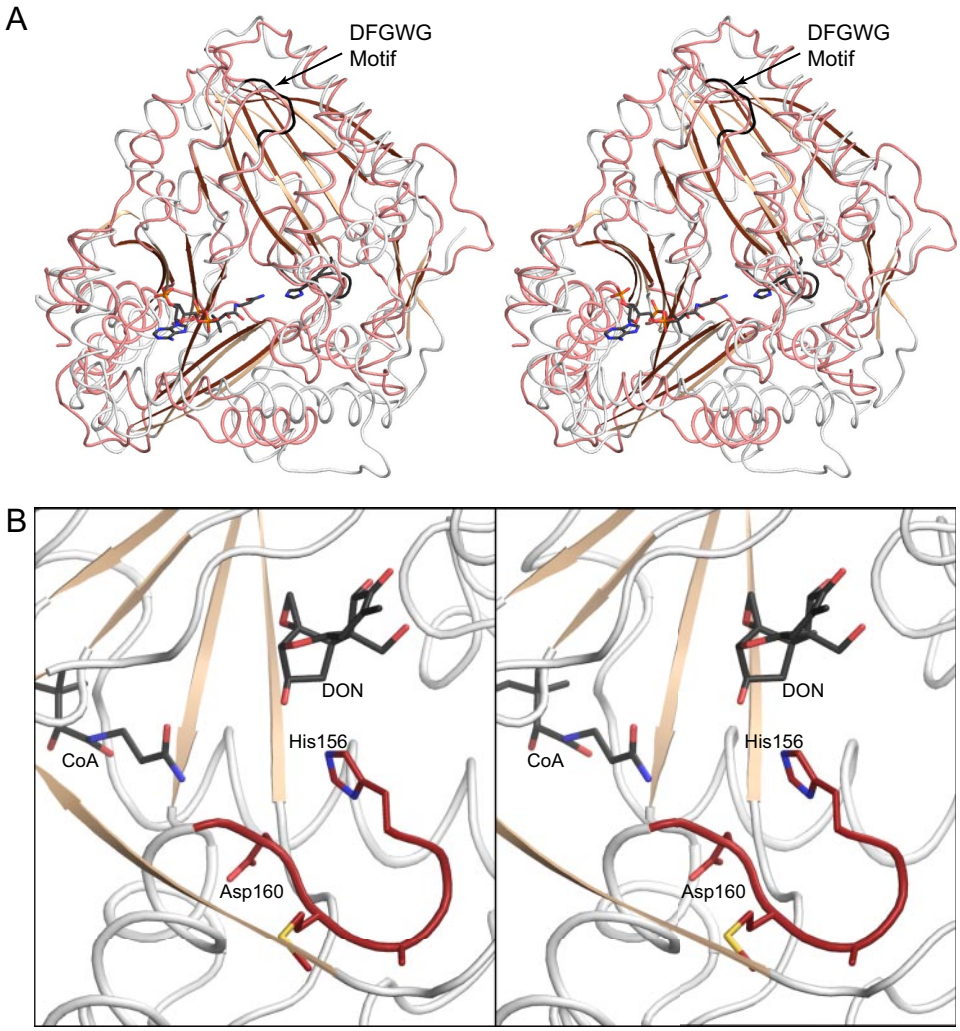

FIGURE 3. **Stereo superposition of FgTRI101 and vinorine synthase and the environment of the HX_3D motif.** In *A*, FgTRI101 is depicted in *white* with its β-strands colored in *wheat*. Vinorine synthase is depicted in *light blue* with its β-strands colored in *dark blue*. HX_3D and DFGWD motifs for FgTRI101 are depicted in *dark gray*. As seen the HX_3D motif lies deep within the hole that extends from one face of the molecule to the other where the catalytic histidine is clearly visible. In contrast, the DFGWD motif is associated with the domain swapped β-strand and appears to play a structural rather than catalytic role. CoA from FgTRI101 is included as a reference marker for the location of the active site. *Panel B* shows a closeup view of the HX_3D motif in FgTRI101 relative to CoA and DON. The motif is depicted in *dark red*. This shows that the conserved aspartate Asp^{160} does not interact with either CoA or the trichothecene and appears to play a structural role in the active site. The coordinates for vinorine synthase were obtained from the RCSB (accession number 2BGH) (32).

ternary complexes of FgTRI101 and FsTRI101 bound to CoA and T-2 have been determined. Comparisons of the apo FgTRI101 structure with the binary and ternary substrate-bound complexes show no large scale domain movements upon substrate binding. The root mean square differences between the apo FgTRI101 and all of its complexes are less than 0.36 Å for at least 368 α-carbon atoms. Likewise, the tertiary structures of the FgTRI101 and FsTRI101 ternary complexes bound to CoA·T-2 are very similar, where 391 structurally equivalent α-carbon atoms can be superimposed with root mean square differences of 0.46 Å. The structure of TRI101 is discussed in the context of FgTRI101.

The tertiary structure of FgTri101 consists of an N-terminal and C-terminal domain (Fig. 2) that associate to form a doughnut-shaped protein. The active site lies in the doughnut-hole that is formed by the interface between these domains. The N-terminal domain belongs to the α/β class and is composed of two mixed β-sheets with three and five strands each (the topology of TRI101 is defined in supplemental Fig. 1). The three-stranded β-sheet (β-1,3,4) is on the surface of the protein distal from the base of the active site cleft. This sheet does not participate in the domain interface or ligand binding. The five-stranded β-sheet is composed of four N-terminal domain strands (β-2,5,6,7) and one domain swapped strand (β-12) from the C-terminal domain. Packed on both faces of the five-stranded β-sheet are seven α-helices, six are from the N-terminal domain (α-1,2,3,4,5,6), and α-14 is contiguous with the domain swapped β-12 strand. The proposed catalytic histidine (FgHis^{156}) is located in the loop between β-7 and α-5 at the interface of the two domains.

The C-terminal domain contains a seven-stranded mixed β-sheet (β-8,9,10,11,13,14,15) that forms a substantial part of the interface between the domains. Seven α-heli-

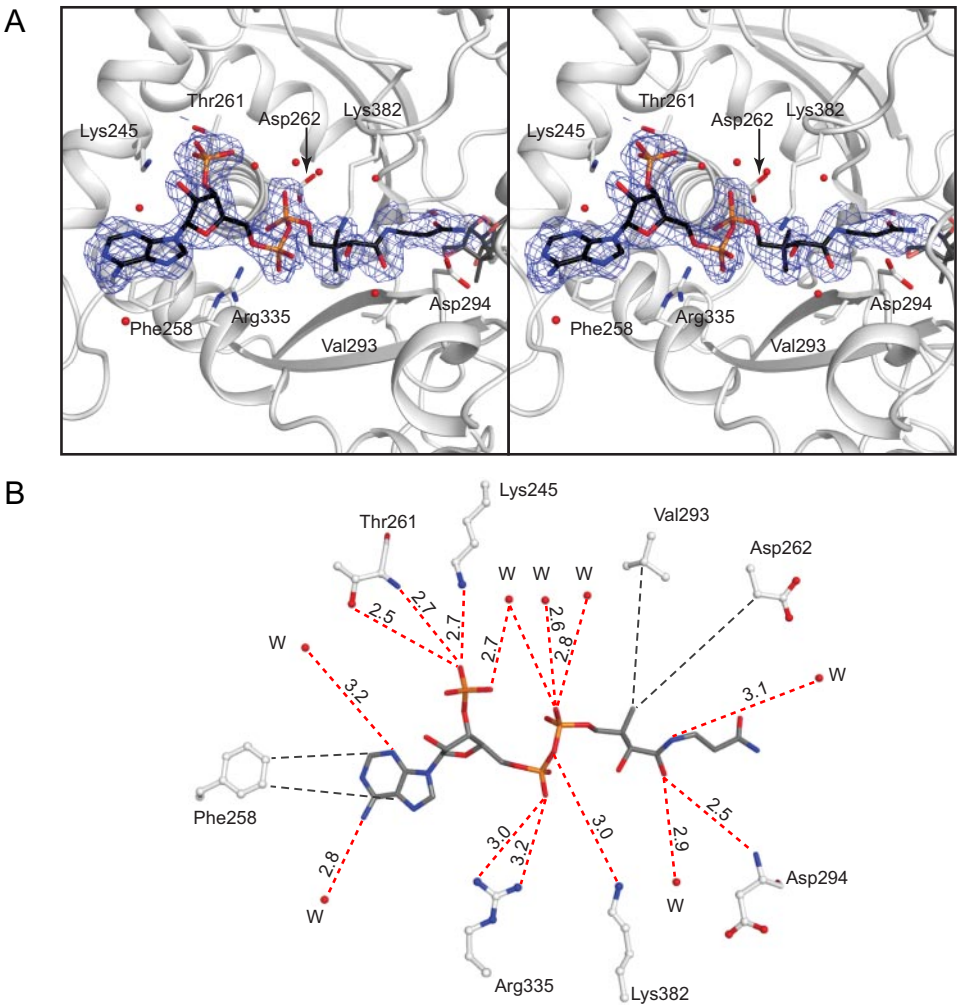

FIGURE 4. **Stereoview of the electron density for CoA and T-2 in their complex with FgTRI101 at 1.6 Å resolution and a schematic ligand interaction diagram.** *A*, the electron density map, contoured at 3σ was calculated from coefficients of the form $F_o - F_c$ where the ligand was omitted from the phase calculation and refinement. Lys^{382} adopts two conformations where only one of these interacts with CoA. Only this conformation is shown. The ligand interaction diagram shown in *B* was derived from a calculation with LIGPLOT (40) and displayed utilizing Pymol.

ces (α-8,9,11,12,15,16) are packed against the exterior face of this β-sheet, whereas two α-helices (α-10,13) contribute to the interface between the two domains.

A search for structurally homologous proteins utilizing the DALI server shows that TRI101 is most similar to the acetyltransferase vinorine synthase, where 317 structurally equivalent α-carbon atoms superimpose with a root mean square difference of 1.82 Å, even though they only share 18% sequence identity (RCSB accession number 2BGH (32)). A superposition of FgTRI101 and vinorine synthase is shown in Fig. 3.

Vinorine synthase is a member of a larger group of enzymes that catalyze acyl transfer reactions. These have been referred to as the BADH family of enzymes where the acronym is based on the first four members to be identified. This group includes anthocyanin malonyltransferase and phthiocerol dimycocerosyl transferase for which structures are also known (33, 34). They exhibit similar topologies and have two conserved sequence motifs, a catalytically important HX_3D and a structurally important DFGWG motif (35). Superposition of FgTRI101 with vinorine synthase reveals that the conserved motifs are in structurally equivalent positions. The role of these motifs is discussed in the context of the active site.

Quaternary Structure—The two orthologs of TRI101 exhibit different oligomeric states in both the crystal lattice and solution. FsTRI101 crystallized with four monomers in the asymmetric unit where examination of the lattice shows that these form two loosely assembled dimers with similar interfaces. The common interface buries 530 Å^2 surface area per monomer where a substantial proportion of the buried surface area is provided by interactions between 2-fold related purine rings of CoA on adjacent subunits. The surface area is 40% hydrophobic, as calculated by SurfRacer (36). The small size of the interface and the low percent of hydrophobic residues suggest that FsTRI101 is not a dimer in solution as was confirmed by gel filtration (data not shown). In contrast, for FgTRI101 there is one molecule in the asymmetric unit, but the crystal packing suggests that protein exists as a dimer. In that lattice two molecules related by a crystallographic 2-fold axis bury a surface area of 690 Å^2 per subunit where the interface is 70% hydrophobic. Gel filtration analysis revealed that in solution FgTRI101 consists of a mixed population of monomers and dimers (data not shown). The significance of this monomer-dimer equilibrium relative to the kinetic properties of the enzyme is not known.

Active Site—The active site for TRI101 was identified by the location of the electron density for CoA and the trichothecene mycotoxins used in this study (Figs. 4 and 5 and supplemental Fig. 2). In the case of FgTRI101 bound to DON and T-2 the electron density was unequivocal and close to an occupancy of 1.0. For the complex of FsTRI101 with T-2 the occupancy appeared to be closer to 0.6, but the overall orientation of the substrate was still clearly evident (supplemental Fig. 2). In all cases the electron density for the trichothecene ligands was unequivocal. CoA was clearly defined except for the terminus of the β-mercaptoethylamine moiety that showed weak occupancy in the crystal structures and was only modeled into the FsTRI101·CoA·T-2 structure. The binding site for CoA is associated mostly with the N-terminal domain. The binding mode is similar to that seen for other carnitine acyltransferases (PDB 2BGH and 1Q9J) (29, 31). The adenosine portion is solvent exposed, whereas the pantothenic acid and β-mercaptoethylamine moieties adopt an extended conformation and extend

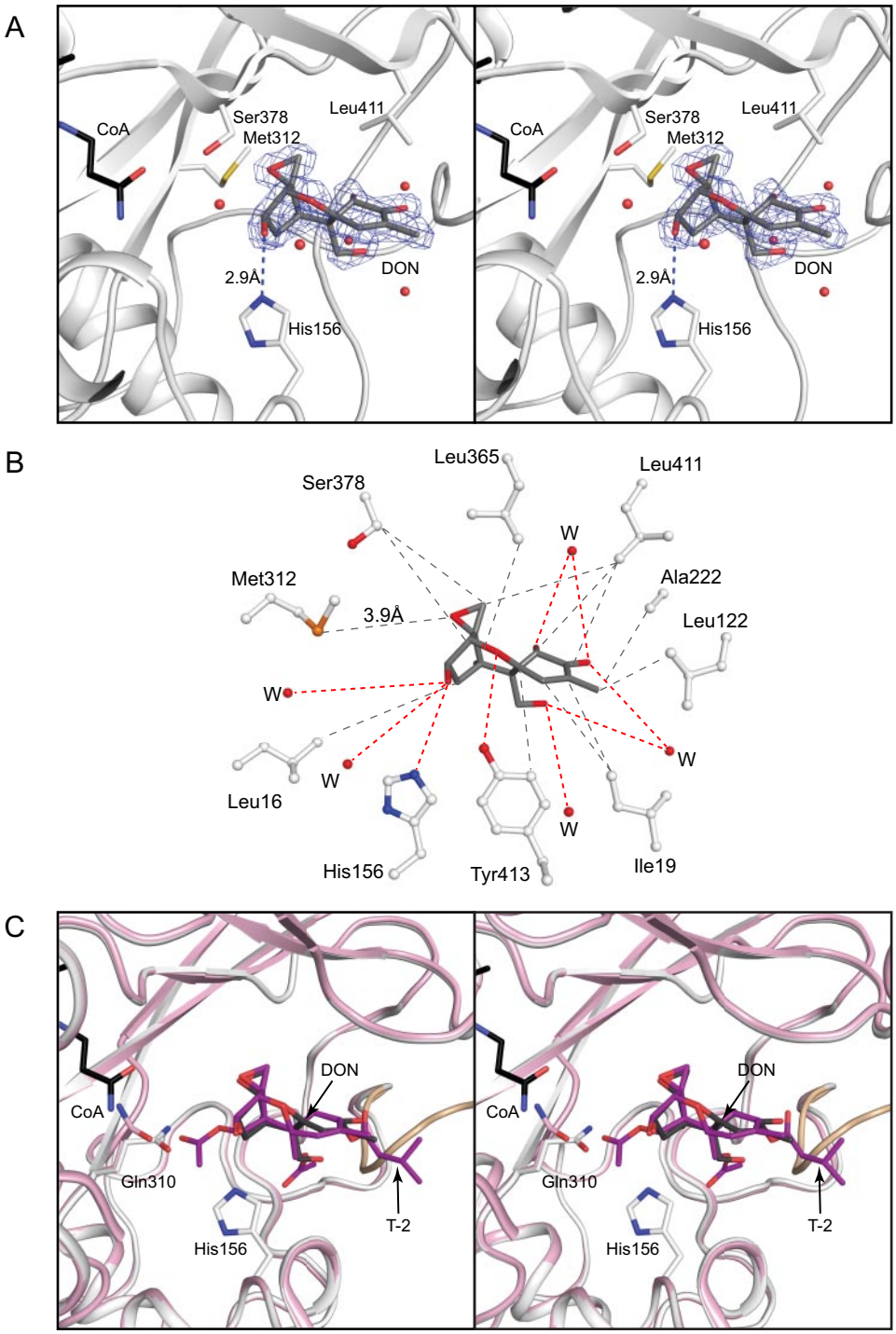

FIGURE 5. **Details of the interaction of mycotoxin DON and T-2 with FgTRI101.** *A* presents a stereoview of the electron density corresponding to DON bound to FgTRI101. The map, contoured at 3σ was calculated from coefficients of the form $F_o - F_c$ where the ligand was omitted from the phase calculation and refinement. Residues that interact with the epoxide moiety are depicted as *sticks*. *B* shows a schematic diagram of the interactions between DON and FgTRI101. *C* reveals the differences in the active site induced by the binding of T-2 compared with DON. FgTRI101 in the complex with T-2 is depicted in *pink*, whereas FgTRI101 in the complex with DON is depicted in *white*. The ordered loop between $FgGly^{219}$ and $FgThr^{225}$ in the complex with DON is depicted in *wheat*. As noted in the text, Gln^{310} rotates to accommodate the acetyl group on C4 of the trichothecene substrate T-2. The ligand interaction diagram shown in *B* was derived from a calculation with LIGPLOT (40) and displayed utilizing Pymol.

into the active site pocket through a narrow tunnel. In contrast, the trichothecene binding site lies in a large cavity on the opposite side of the enzyme from the CoA binding site but likewise projects its 3-hydroxyl group into the tunnel that extends through the enzyme. The position of the bound CoA would place the acetyl group of acetyl-CoA in close proximity to both the substrate and the catalytic histidine.

The HX_3D motif is located so that the histidine residue is available to both the acetyl-CoA and substrate binding sites. Both the histidine and aspartate residues of this motif have previously been shown to be critical for catalysis in vinorine synthase (37). Whereas the histidine residue is ideally positioned between CoA and the trichothecene mycotoxins to function as the catalytic base, the role of the aspartate residue in this motif is less clear. In FsTRI101, FgTRI101, and vinorine synthase the aspartate residue is directed away from the substrates, forming a salt bridge with an arginine residue while also serving as a capping residue for the succeeding α-helix (Fig. 3*b*). This suggests that this conserved residue performs a structural role within the active site.

In contrast, the DFGWG ($FgAsp^{389}$ . . .) motif is not located near the active site, rather it is a component of the domain swapped loop preceding β12. Furthermore, in the TRI101 orthologs this motif is not strictly conserved, where the fourth position is either a Phe/Leu as observed in FsTRI101 and FgTRI101, respectively. A sequence alignment of functional trichothecene 3-*O*-acetyltransferases identified this as a conserved motif among *Fusarium* species (38). The structural data suggest that the variable fourth position may simply require a large hydrophobic group for anchoring the turn of the domain swapped loop. This suggests that the DFG*X*G motif plays an important structural role.

Trichothecene Binding Site—The trichothecene binding pocket is located on the opposite face of the molecule relative to CoA (Fig. 5). As noted above, the catalytic histidine of the HX_3D conserved motif is ideally positioned for base-catalyzed abstraction of the proton from the C3 hydroxyl group of DON. The trichothecene binding interactions, as exemplified by the structure of DON bound to FgTRI101, are largely hydrophobic. The epoxide moiety is

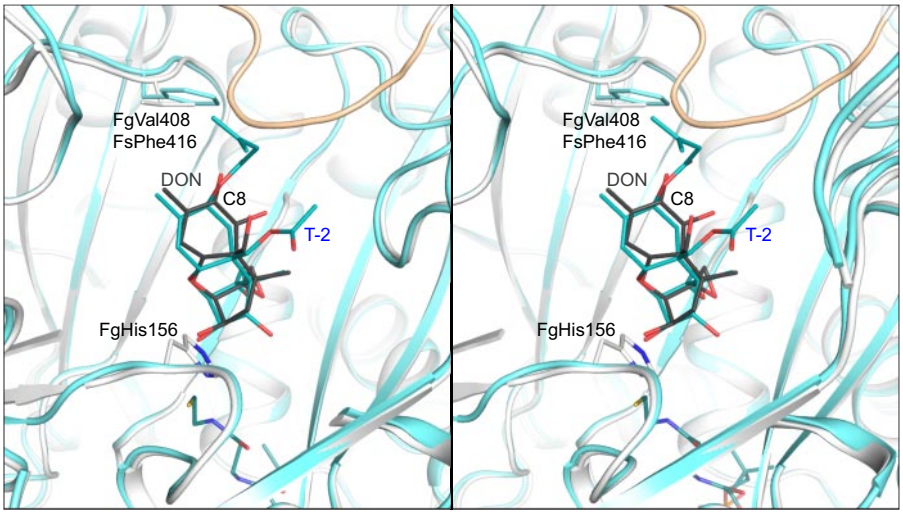

FIGURE 6. **Stereo overlay of ternary complexes of FsTRI101·CoA·T-2 and FgTRI101·CoA·DON.** FgTRI101 is depicted in *white* except for the loop between FgGly^{219} and FgThr^{225}, which is colored in *wheat*. DON is colored in *dark gray*. FsTRI101 is depicted in *cyan* where CoA and T-2 are colored in *teal*. The C8 carbonyl oxygen of DON is oriented toward FgVal^{408} where this residue is a phenylalanine in FsTRI101 (FsPhe^{416}). This location is proposed to be a determinant of substrate specificity in these orthologs. For clarity, residues FgGln^{12}–FgTyr^{20} and FgVal^{60}–FgGlu^{63} together with the structurally equivalent residues in FsTRI101 were omitted from the figure.

inserted into a hydrophobic cavity formed by residues from four adjacent strands of the central β sheet and the connecting loopsof the C-terminal domain. The sulfur atom of FgMet^{312} is positioned 3.9 Å from the epoxide oxygen, whereas the methylene carbon is in close proximity to FgLeu^{411} (3.6 Å). This hydrophobic environment most likely serves to protect the epoxide from hydrolysis. The coordination site for DON also includes seven hydrogen bonds, two from side chain residues and the remainder from waters trapped in the active site (Fig. 5).

Superposition of the structures for FgTRI101 bound to DON and T-2, respectively, show that, although most of the binding site exhibits the same conformation, there are two important changes. First the loop that includes residues FgGly^{220} and FgPro^{226} that is ordered in the complex with DON is disordered in the presence of T-2. Second, FgGLn^{310} rotates to increase the volume of the binding pocket at the position complementary to the trichothecene C4 position. The superposition shows that the isovaleryl group of T-2 at C8 and the acetyl group at C15 would cause a steric collision with this loop if it adopted the same conformation as observed in the presence of DON (Fig. 5*c*). Likewise, Gln^{312} rotates to accommodate the acetyl group at C4 in T-2 that is absent in DON. This provides a measure of the plasticity of the active site that allows it to accommodate a range of trichothecenes substrates.

Structural Comparison of FgTRI101 and FsTRI101—Comparison of the structures and sequences for FgTRI101 and FsTRI101 shows that the residues that line the toxin binding site are identical except for a surface flexible loop and a hydrophobic residue adjacent to the trichothecene C8 position (Fig. 6). The surface loop is located between FsPro^{224} and FsPro^{234} and is disordered in the FsTRI101·CoA·T-2 complex. Interestingly this section contains four proline residues whose role in specificity is uncertain. The structurally equivalent residues in FgTRI101 are FgPro^{215}-FgPro^{226}, which include the shorter section of FgTRI101 that is disordered in its complex with T-2 but ordered in the presence of DON. The ordered loop in FgTRI101 partly blocks the toxin active site from solvent and is in close proximity to the C8 ketone oxygen of the toxin (<3.5 Å), but this loop does not form any direct polar interactions with the bound DON mycotoxin. Superposition of the FgTRI101·CoA·T-2 structure onto the DON-bound structure shows that the isovaleryl group of T-2 would cause a steric collision with this flexible loop if it were to adopt a conformation similar to that observed in FgTRI101 complexed with DON. The role of this loop in substrate specificity in both enzymes is unclear because it is disordered in the presence of Type A toxins, but it is reasonable to assume that it contributes to the ability of these enzymes to accommodate a range of substrates.

The second difference in the toxin binding site between orthologs is the identity of a hydrophobic residue positioned adjacent to the chemical group associated C8 of the trichothecene. FgVal^{408} and FsPhe^{416} both form a hydrophobic interaction with the C8 isovaleryl group of bound T-2. However, in DON, there is a ketone moiety at C8 and the DON bound structure of FgTRI101 shows that Val^{408} is too short to interfere with DON binding. Attempts to obtain a FsTRI101 structure with DON bound were unsuccessful, but a superposition of the FgTRI101·CoA·DON structure onto the FsTRI101·CoA·T-2 structure shows that the C8 ketone of DON would be pointed toward the Cζ atom of FsPhe^{416} at a distance of 3.9 Å (Fig. 6). The difference in the active site architecture at this position, coupled with the large increase in K_m for substrates with a ketone at C8 (described below) support that FsPhe^{416} is a determinant of catalytic efficiency for FsTRI101. These differences are most likely responsible for the differences in kinetic parameters discussed later.

Proposed Mechanism—Based on the position and orientation of FgHis^{156} relative to the C3 hydroxyl group, together with the structural homology to other acyltransferase family members, the following mechanism is proposed for the acetyl transfer reaction of TRI101. The catalytic histidine, FgHis^{156}, abstracts a proton from the C3 hydroxyl group of the trichothecene substrate. Thereafter the deprotonated oxygen at the toxin C3 position nucleophilically attacks the carbonyl carbon of acetyl-CoA forming a tetrahedral intermediate. Decomposition of the tetrahedral intermediate into an acetylated toxin and CoA requires the donation of a proton from a proton donor. Water molecules were observed in the active site in close proximity to the C3 hydroxyl, but are unlikely to be the proton donor as there are appropriate residues nearby that might serve to reduce the pK_a of a water molecule. The composition of the active site suggests that the proton donor is most likely the catalytic FgHis^{156}, thereby resetting the active site for another round of catalysis (Fig. 7).

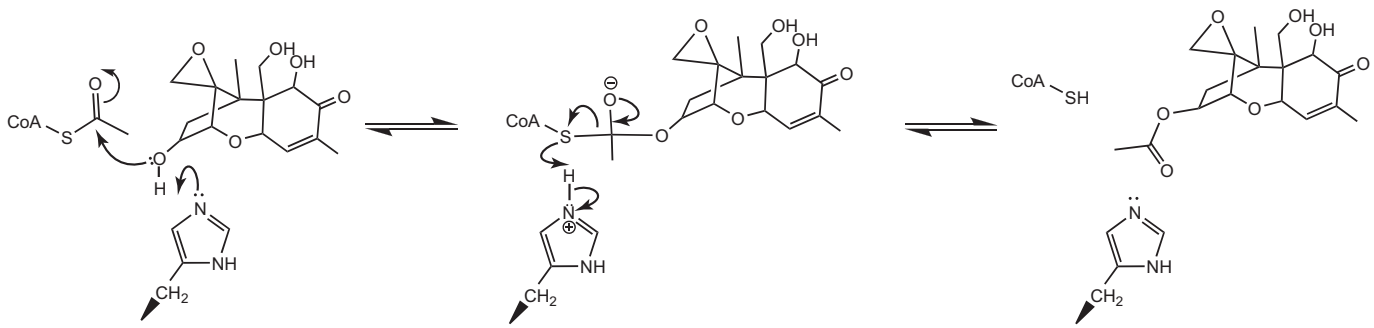

FIGURE 7. **Proposed mechanism for the TRI101 acetyltransferase reaction.**

TABLE 2

Kinetic constants, K_m and k_{cat}, for FsTRI101 and FgTRI101 with trichothecene mycotoxins

Ortholog	Toxin	K_m	k_{cat}	k_{cat}/K_m
		μM	s^{-1}	$M^{-1} \times s^{-1}$
FsTRI101	Isotrichodermol	17.1 ± 1.1	127 ± 6.6	7.4×10^6
FgTRI101	Isotrichodermol	10.2 ± 3.5	411 ± 93	4.0×10^7
FsTRI101	T-2	15.8 ± 2.6	103 ± 64	6.5×10^6
FgTRI101	T-2	3.9 ± 0.6	14 ± 2.2	3.6×10^6
FsTRI101	DON	1463 ± 425	28 ± 3.6	1.7×10^4
FgTRI101	DON	11.7 ± 3.5	13.5 ± 2.1	1.2×10^6
FsTRI101	NIV	350 ± 33	85 ± 9.6	2.4×10^5
FgTRI101	NIV	47 ± 6.8	443 ± 23	9.4×10^6

Kinetic Analysis of FsTRI101 and FgTRI101—Previous studies have demonstrated that TRI101 isolated from different trichothecene producing organisms are able to acetylate both A and B type trichothecene mycotoxins (13, 18, 20, 21, 38). However, these earlier studies were limited to end point assays that did not evaluate the catalytic rate of each ortholog. Here a chemically coupled assay has been utilized to follow the rate of production of CoA generated by acetyl transfer to the toxin substrate. With this assay, the K_m and k_{cat} values for FsTRI101 and FgTRI101 with the native substrate, isotrichodermol, and three agriculturally important trichothecene mycotoxins, T-2, DON, and NIV, were determined. The kinetic constants, K_m and k_{cat}, are presented in Table 2.

With isotrichodermol as substrate, FsTRI101 and FgTRI101 are efficient enzymes whose k_{cat}/K_m values differ only by a factor of 5 in favor of FgTRI101. Analysis of an A type trichothecene (T-2) showed that the K_m of this substrate was not significantly elevated for either orthologs and although the catalytic efficiencies are somewhat lower these are the same within the margin of error. This is surprising given that there is substantial modification of the core ring when comparing T-2 to isotrichodermol (Fig. 1). In contrast, the orthologs exhibit significantly different activities toward B type trichothecenes (DON and NIV). The most surprising result is the large reduction in the efficiency of FsTRI101 for DON. The K_m is increased 85 times and the k_{cat}/K_m is reduced by a factor of 435 when compared with isotrichodermol. In contrast, the K_m for FgTRI101 with DON remains essentially unchanged and the k_{cat}/K_m is decreased by 1 order of magnitude and shows a similar efficiency to that seen for T-2 with this enzyme. Comparing the kinetic parameters for FsTRI101 to FgTRI101, FsTRI101 exhibits an ~130 times greater value for K_m and 70 times lower value for the catalytic efficiency. These substantial differences are surprising given that DON is a relatively unsubstituted trichothecene. This suggests that there is a specific difference between these enzymes that allows FgTRI101 to efficiently acetylate a broader range of substrates relative to FsTRI101.

Enzyme Activity Determinants—The kinetic analysis identified two striking features in the activity for the two TRI101 orthologs analyzed: both orthologs do not differ significantly in their catalytic efficiency for the initial substrate in the biosynthetic pathway (isotrichodermol) compared with the highly decorated trichothecenes such as T-2. In contrast, the catalytic efficiency of the FsTRI101 ortholog is decreased substantially for B type trichothecenes. The small differences in catalytic efficiency between isotrichodermol and A type trichothecenes is difficult to explain given the large changes in the decoration of the mycotoxin core. Clearly, the flexible loops that include residues G^{220}DAVLTP^{226} in FgTRI101 and P^{224}APAGDAPPAla^{233} in FsTRI101 are important contributors to the ability to accept different substrates. This is exemplified by order-disorder transition seen in the binding of T-2 relative to DON. Indeed, without this transition it is difficult to see how the active site could accommodate a trichothecene with a large substituent at C15 and C8.

In the absence of a structure for DON bound to FsTRI101 it is difficult to unequivocally set forward a structural model that will account for the kinetic difference toward this substrate. It is conceivable that the identity of the hydrophobic residue positioned proximal to the toxin C8 ketone influences the activity. This residue is a valine in FgTRI101 and a phenylalanine in FsTRI101. The ternary structure of FgTRI101·CoA·DON superposed onto FsTRI101·CoA·T-2 shows that the binding orientation of DON and T-2 is almost identical between orthologs. Importantly, binding of B type trichothecenes would direct the C8 ketone toward the Cζ of $FsPhe^{416}$ at a distance of 3.9 Å. This distance and orientation might create an unfavorable interaction, resulting in the reduced catalytic efficiency of B type trichothecenes that were observed. Examination of a sequence alignment for functional trichothecene 3-*O*-acetyltransferases at this position suggests that a hydrophobic residue larger than valine results in reduced activity toward DON (38) (see supplemental Fig. S3).

Conclusions—This study shows that there are significant differences in the kinetic ability of TRI101 orthologs to inactivate trichothecene mycotoxins. It is anticipated that these differences might be reflected in the ability of these enzymes to combat *Fusarium* head blight when inserted as transgenes and hence the choice of enzyme may be critical. The flexible loop

between FgPro^{215}–FgPro^{226} and the size of the hydrophobic residue at FgVal^{408} are proposed to be important determinants of catalytic efficiency and a mutational analysis to investigate the role of each residue is in progress. The kinetic results suggest that the FHB disease resistance in the field to DON mycotoxin producing strains of *Fusarium* could be improved by using a TRI101 ortholog from *F. graminearum*. This ortholog has a 70-fold greater *in vitro* k_{cat}/K_m with DON compared with FsTRI101. Conversely, it might be expected that TRI101 from *F. sporotrichioides* would provide more resistance to T-2 than DON *in planta.* Experiments to test these hypotheses are in progress.

Acknowledgments—We thank Dr. Martin St. Maurice for helpful discussion of the kinetic studies and Kirsten Dennison for plasmid construction.

REFERENCES

1. Nganje, W. E., Bangsund, D. A., Leistritz, F. L., Wilson, W. W., and Tiapo, N. M. (2004) *Rev. Agric. Econom.* **26,** 332–347
2. Pestka, J. J., and Smolinski, A. T. (2005) *J. Toxicol. Environ. Health* **8,** 39–69
3. Kim, H. S., Lee, T., Dawlatana, M., Yun, S. H., and Lee, Y. W. (2003) *Mycol. Res.* **107,** 190–197
4. Larsen, J. C., Hunt, J., Perrin, I., and Ruckenbauer, P. (2004) *Toxicol. Lett.* **153,** 1–22
5. Cundliffe, E., Cannon, M., and Davies, J. (1974) *Proc. Natl. Acad. Sci. U. S. A.* **71,** 30–34
6. Ueno, Y., Sawano, M., and Ishii, K. (1975) *Appl. Microbiol.* **30,** 4–9
7. Anderson, D. W., Black, R. M., Lee, C. G., Pottage, C., Rickard, R. L., Sandford, M. S., Webber, T. D., and Williams, N. E. (1989) *J. Med. Chem.* **32,** 555–562
8. Kimura, M., Shingu, Y., Yoneyama, K., and Yamaguchi, I. (1998) *Biosci. Biotechnol. Biochem.* **62,** 1033–1036
9. McCormick, S. P., Alexander, N. J., and Proctor, R. H. (2006) *Can. J. Microbiol.* **52,** 636–642
10. Tokai, T., Koshino, H., Takahashi-Ando, N., Sato, M., Fujimura, M., and Kimura, M. (2007) *Biochem. Biophys. Res. Commun.* **353,** 412–417
11. Hohn, T. M., and Vanmiddlesworth, F. (1986) *Arch. Biochem. Biophys.* **251,** 756–761
12. Rynkiewicz, M. J., Cane, D. E., and Christianson, D. W. (2001) *Proc. Natl. Acad. Sci. U. S. A.* **98,** 13543–13548
13. Kimura, M., Kaneko, I., Komiyama, M., Takatsuki, A., Koshino, H., Yoneyama, K., and Yamaguchi, I. (1998) *J. Biol. Chem.* **273,** 1654–1661
14. McCormick, S. P., and Alexander, N. J. (2002) *Appl. Environ. Microbiol.* **68,** 2959–2964
15. Alexander, N. J., McCormick, S. P., and Hohn, T. M. (1999) *Mol. Gen. Genet.* **261,** 977–984
16. Poppenberger, B., Berthiller, F., Lucyshyn, D., Sieberer, T., Schuhmacher, R., Krska, R., Kuchler, K., Glossl, J., Luschnig, C., and Adam, G. (2003) *J. Biol. Chem.* **278,** 47905–47914
17. Shima, J., Takase, S., Takahashi, Y., Iwai, Y., Fujimoto, H., Yamazaki, M., and Ochi, K. (1997) *Appl. Environ. Microbiol.* **63,** 3825–3830
18. McCormick, S. P., Alexander, N. J., Trapp, S. E., and Hohn, T. M. (1999) *Appl. Environ. Microbiol.* **65,** 5252–5256
19. Muhitch, M. J., McCormick, S. P., Alexander, N. J., and Hohn, T. M. (2000) *Plant Sci.* **157,** 201–207
20. Okubara, P. A., Blechl, A. E., McCormick, S. P., Alexander, N. J., Dill-Macky, R., and Hohn, T. M. (2002) *Theor. Appl. Genet.* **106,** 74–83
21. Manoharan, M., Dahleen, L. S., Hohn, T. M., Neate, S. M., Yu, X. H., Alexander, N. J., McCormick, S. P., Bregitzer, P., SchwarZ, P. B., and Horsley, R. D. (2006) *Plant Sci.* **171,** 699–706
22. Ohsato, S., Ochiai-Fukuda, T., Nishiuchi, T., Takahashi-Ando, N., Koizumi, S., Hamamoto, H., Kudo, T., Yamaguchi, I., and Kimura, M. (2007) *Plant Cell Rep.* **26,** 531–538
23. Shih, Y. P., Wu, H. C., Hu, S. M., Wang, T. F., and Wang, A. H. (2005) *Protein Sci.* **14,** 936–941
24. Atlas, R. (1995) *Handbook of Media for Environmental Microbiology*, CRC Press, Boca Raton, FL
25. Otwinowski, Z., and Minor, W. (1997) *Methods Enzymol.* **276,** 307–326
26. Terwilliger, T. C., and Berendzen, J. (1999) *Acta Crystallogr. Sect. D Crystallogr.* **55,** 849–861
27. Terwilliger, T. C. (2000) *Acta Crystallogr. D Biol. Crystallogr.* **56,** 965–972
28. Emsley, P., and Cowtan, K. (2004) *Acta Crystallogr. D Biol. Crystallogr.* **60,** 2126–2132
29. Murshudov, G. N., Vagin, A. A., and Dodson, E. J. (1997) *Acta Crystallogr. D Biol. Crystallogr.* **53,** 240–255
30. Vagin, A., and Teplyakov, A. (2000) *Acta Crystallogr. D Biol. Crystallogr.* **56,** 1622–1624
31. Ellman, G. L. (1959) *Arch. Biochem. Biophys.* **82,** 70–77
32. Ma, X., Koepke, J., Panjikar, S., Fritzsch, G., and Stockigt, J. (2005) *J. Biol. Chem.* **280,** 13576–13583
33. Unno, H., Ichimaida, F., Suzuki, H., Takahashi, S., Tanaka, Y., Saito, A., Nishino, T., Kusunoki, M., and Nakayama, T. (2007) *J. Biol. Chem.* **282,** 15812–15822
34. Buglino, J., Onwueme, K. C., Ferreras, J. A., Quadri, L. E., and Lima, C. D. (2004) *J. Biol. Chem.* **279,** 30634–30642
35. D'Auria, J. C. (2006) *Curr. Opin. Plant Biol.* **9,** 331–340
36. Tsodikov, O. V., Record, M. T., Jr., and Sergeev, Y. V. (2002) *J. Comput. Chem.* **23,** 600–609
37. Bayer, A., Ma, X., and Stockigt, J. (2004) *Bioorg. Med. Chem.* **12,** 2787–2795
38. Tokai, T., Fujimura, M., Inoue, H., Aoki, T., Ohta, K., Shibata, T., Yamaguchi, I., and Kimura, M. (2005) *Microbiology* **151,** 509–519
39. DeLano, W. L. (2002) *The PyMOL Molecular Graphics System*, DeLano Scientific LLC, San Carlos, CA
40. Wallace, A. C., Laskowski, R. A., and Thornton, J. M. (1995) Protein Eng. **8,** 127–134